



# Construction of polythiophene-derivative films as a novel electrochemical sensor for highly sensitive detection of nitrite

Yanping Li<sup>1</sup> · Chao Geng<sup>1</sup> · Xiaoyun Xu<sup>1</sup> · Xiaoyi Lv<sup>1</sup> · Yishan Fang<sup>1</sup> · Na Wang<sup>1</sup> · Yunjun Yang<sup>2</sup> · Bo Cui<sup>1</sup>

Received: 13 July 2021 / Revised: 8 August 2021 / Accepted: 19 August 2021 / Published online: 30 September 2021  
© Springer-Verlag GmbH Germany, part of Springer Nature 2021

## Abstract

Herein, a novel, convenient, and highly selective electrochemical sensor for determination of nitrite based on a polythiophene-derivative film-modified glassy carbon electrode (GCE) was established. In this work, 2,5-di-thiophen-3-yl-thiazolo[5,4-d]thiazole (DTT), a novel thiophene derivative, was synthesized and used to form an original and excellent polymer film (PolyDTTF) on GCE through one-step electropolymerization for the first time. The modified electrodes were characterized by electron microscopy (SEM), Fourier transform infra-red spectroscopy (FT-IR), UV-visible spectra, Raman spectroscopy, and electrochemical technologies, in which the electrochemical sensor based on PolyDTTF was successfully constructed and demonstrated a significant electrocatalytic effect on nitrite. The influence of pH value, electrodeposition scanning times, scanning speed, and potential on the electrochemical behavior of nitrite were investigated in detail. Furthermore, the nitrite sensor exhibits excellent responses proportional to nitrite concentrations ( $R^2 = 0.9972$ ) over a concentration range of  $5.5 \times 10^{-9} \sim 3.5 \times 10^{-5}$  M with a detection limit (LOD) of 2 nM, and has extremely good anti-interference ability for nitrite detection. This proposed sensor can be used to detect nitrite in actual samples, opening the possibility for applications in the food industry and environmental analysis.

**Keywords** PolyDTTF · Electropolymerization · Modified electrode · Electrochemical analysis · Nitrite sensing

## Introduction

As the primary source of nitrogen for green plants, nitrite is the most common nitrogenous compound found in nature, and it is widely used in drinking water and food. It can not only make food present a good color and luster, and enhance people's appetite for food, but also prevent food from rotting and deteriorating, thereby increasing the flavor of food [1, 2]. However, when it is used improperly or excessively during

processing, nitrite will cause adverse effects on human health through the blood. It could combine with blood pigments to produce methemoglobin, which no longer needs oxygen in tissues, or interacts with amines and amides in the stomach to form highly carcinogenic N-nitrosamine compounds [3–5]. Because of the potential toxicity of nitrite to the human body, the development of a rapid and sensitive nitrite detection technology is of great significance to public health.

Currently, many analytical techniques have been proposed for nitrite detection, such as spectrophotometry [6–9], colorimetry [10], capillary electrophoresis [11–13], chromatography [14–16], chemiluminescence [17, 18]. Nevertheless, most of the reported detection techniques involve some defects, such as expensive cost, limited selectivity, slow detection speed, and low sensitivity [2, 19]. By contrast, in practical application, electrochemical analysis technology has received great attention in nitrite determination because of its simple preparation, low cost, high sensitivity and easy miniaturization [20, 21]. At present, the quality and safety of food are highly valued, and the sensitive detection of nitrite in food is of great significance to the health of the general public.

Up to now, our interest has been focused on the introduction of various indicator molecules as electrode modifiers in nitrite

✉ Yishan Fang  
fangysh123@qlu.edu.cn

✉ Yunjun Yang  
yyj@qlu.edu.cn

✉ Bo Cui  
cuiibopaper@163.com

<sup>1</sup> State Key Laboratory of Biobased Material and Green Papermaking, School of Food Science and Engineering, Qilu University of Technology, Shandong Academy of Sciences, Jinan 250353, Shandong, China

<sup>2</sup> Academy of Advanced Interdisciplinary Studies, Qilu University of Technology, Shandong Academy of Sciences, Jinan 250353, Shandong, China

sensing, such as polymeric films, a new polyoxometalate/rGO/Pani [22, 23], metal oxides [24], metal chalcogenides [25, 26], metal alloys [27] and carbon nanomaterials [21, 28, 29]. Li et al. proposed a nitrite sensor by using CuO/H-C<sub>3</sub>N<sub>4</sub>/rGO nanocomposite for the nitrite detection [19]. Fan et al. described the construction of cobalt porphyrin/strontium tantalate nanocomposites for nitrite detection [1]. Chen et al. prepared an electrochemical sensing platform based on Cu-MOF, which exhibits high sensitivity as well as satisfied stability for nitrite sensing [2]. Zhang et al. synthesized gold nanoparticles coated on a MoS<sub>2</sub> microsphere for efficient electrochemical sensing of nitrite [30]. However, most of these methods involved complex fabrication and exhibited poor sensitivity and reproducibility. Therefore, it is desirable to establish new strategies to overcome these limitations.

Among them, conductive polymers have attracted great attention in the development of electrochemical sensors due to their inherent conductivity, such as polyaniline, polypyrrole, polythiophene, polyacetylene, and their derivatives, etc. [31]. In this work, a new kind of small molecule material, 2,5-dithiophen-3-yl-thiazolo[5,4-d]thiazole (DTT), was synthesized, and an electrochemical sensing platform based on PolyDTTF-modified glassy carbon electrode (GCE) for the detection of nitrite was established for the first time, where PolyDTTF was prepared through one-step electropolymerization, which is easy to prepare and has controllable film thickness and high environmental stability. DTT is a fused bicyclic heterocyclic compound with rigid planar framework and extended  $\pi$ -conjugated electronic structure [32], while PolyDTTF shows an outstanding catalytic effect for the oxidation of nitrite on account of its high conductivity and excellent catalytic activity. Experimental results displayed that the electrochemical sensor based on PolyDTTF has a preeminent electrocatalytic effect for the determination of nitrite, and it has excellent anti-interference and good stability. This method can be used for the determination of nitrite in actual samples.

## Experimental section

### Reagents and apparatus

Tetrabutylammonium perchlorate was purchased from Shanghai Yuanye Biological Technology Co., Ltd. (China). Potassium ferricyanide and potassium ferrocyanide were obtained from Tianjin Beilian Fine Chemicals Development Co., Ltd. (China). The alumina powder was provided by Shanghai Xianren Instrument Co., Ltd. (China). Sodium nitrite was bought from Tianjin Bodi Chemical Co., Ltd. (China). The ham, sauce beef, and pickle samples were purchased from a local supermarket. The phosphate buffer solutions (PBS) of 0.1 M concentration were prepared using KH<sub>2</sub>PO<sub>4</sub> and K<sub>2</sub>HPO<sub>4</sub>, and the different pHs were adjusted with HCl or

NaOH solution. Other chemical reagents used in this paper were analytical grade, and all aqueous solutions were prepared with ultrapure water from an ultrapure water system. Scanning electron microscopy (SEM, Regulus 8220, Hitachi, Japan) was used for the morphology characterization of the prepared materials. Infrared spectra were measured using a Thermo Fisher Nicolet 10 FTIR spectrometer (Waltham, USA). UV-visible spectra were recorded with a Model TU-1810DSPC spectrometer. A laser confocal Raman spectrometer (Via-Reflex) was used to record the Raman spectrum (2000–400 cm<sup>-1</sup>). The NMR spectra were detected by Bruker AVANCE III instruments (Karlsruhe, Germany) at 100 MHz and 400 MHz for <sup>1</sup>H NMR and <sup>13</sup>C NMR. All electrochemical measurements were implemented with a CHI model 660E potentiostat (CH Instruments, Shanghai, China).

### Preparation of DTT conductive polymer

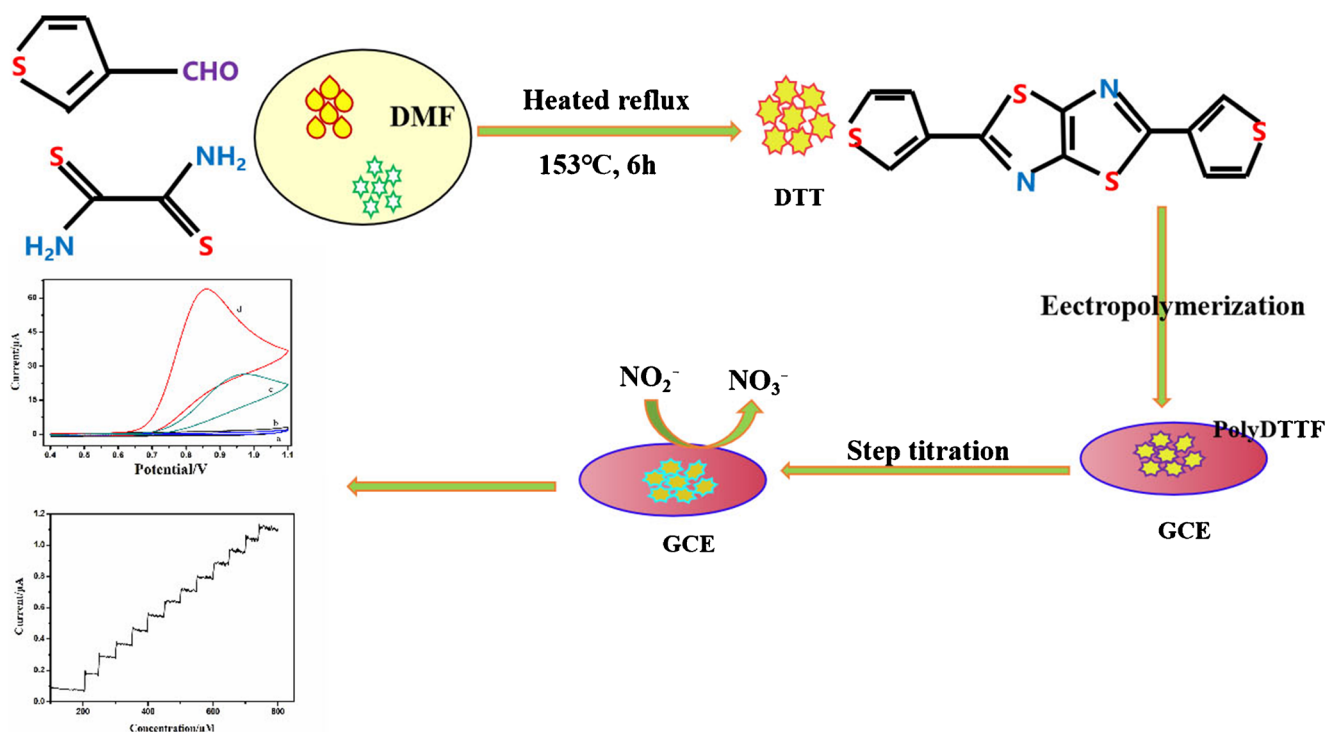
DTT was prepared based on a previous literature with some modification [33]. A solution containing 3-thiophenecarboxaldehyde (1.01 g, 9.0 mmol) and dithioamide (0.48 g, 4.0 mmol) in DMF (50 mL) was heated under reflux for 6 h, then cooled down to 80 °C. The reaction mixture was filtered, and washed by DMF and THF. After drying, the product was obtained. Yield: 0.40 g (33%). <sup>1</sup>H NMR (400 MHz, CDCl<sub>3</sub>):  $\delta$  7.58–7.57 (d, 2H), 7.47–7.46 (d, 2H), 7.13–7.10 (t, 2H); <sup>13</sup>C NMR (100 MHz, CDCl<sub>3</sub>):  $\delta$  162.6, 149.8, 137.6, 128.7, 128.1, 126.9.

### Preparation of nitrite sensor

Firstly, the GCE surface was polished twice with 0.3  $\mu$ m aluminum oxide polishing powder to the mirror surface, and ultrasonically washed with ethanol and ultrapure water for 5 min, then rinsed with ultrapure water, and left in ultrapure water for later use. Secondly, the clean electrode was placed in 0.5 M H<sub>2</sub>SO<sub>4</sub> and scanned by cyclic voltammetry at the scanning speed of 0.1 V/s from -1.5 V to 1.5 V until the curve was stable. Thirdly, the above electrode was placed in a solution of 0.06 g/mL DTT (containing 0.1 M tetrabutylammonium perchlorate) in acetonitrile and scanned 35 times with a scanning voltage of -1.6 to 0.2 V and the scanning speed at 1.0 V/s until the current tended to be stable. The preparation of the nitrite sensor is schematically illustrated in Scheme 1.

### Electrochemical measurements

The cyclic voltammetry (CV), electrochemical impedance spectroscopy (EIS) and amperometric techniques were utilized to investigate the electrochemical activity of the modified electrode. CV measurements were carried out in 0.1 M PBS solution with 2.0 mM K<sub>3</sub>Fe(CN)<sub>6</sub> and 0.1 M KCl, while



**Scheme 1** Schematic illustration for the fabrication and principle of nitrite sensor

CV measurements were also performed in 0.1 M PBS solution without or with 0.1 M nitrite in a potential range of 0.4 ~ 1.1 V and a scan rate of 0.1 V/s. EIS measurements were accomplished in a frequency range between 0.1 kHz and 100 kHz in 0.1 M KCl solution containing 5 mM  $[\text{Fe}(\text{CN})_6]^{3-/4-}$  redox couple. For amperometric measurements, slow magnetic stirring was performed in the electrolytic cell to achieve rapid homogeneity of the analyte solution, and the potential was installed at 0.9 V under experimentally optimized conditions.

### Preparation of actual samples

The samples of ham, sauce beef and pickles were minced in a blender, added with PBS solution and centrifuged at 4000 rpm for 5 min. Then the obtained supernatants were treated with a simple filtration, and the ionic strength and the pH values of the actual sample solution were regulated to match the PBS buffer. Finally, 10  $\mu\text{L}$  of each sample was successively added to the detection system and analyzed for  $\text{NO}_2^-$  content.

## Results and discussion

### Characterization of DTT conductive polymer

The structures of the conducting polymers were characterized using  $^1\text{H}$  NMR and  $^{13}\text{C}$  NMR in Fig. S1, S2 (see Electronic Supplementary Material Fig. S1, S2), which clearly

demonstrated the successful preparation of DTT [34]. The morphology of the polymer film on the surface of the GCE was studied by recording scanning electron microscope images. As represented in Fig. 1a, a brown-black film with some irregular cracks was formed on the surface of the electrode in comparison with bare GCE (Fig. 1a), which fully confirms that the polymer film has been distributed evenly on the surface of the electrode.

Figure 1b shows the Fourier transform infrared spectrum for DTT and PolyDTTF. For DTT, the peak at  $3066\text{ cm}^{-1}$  corresponds to the C-H stretching vibrations of the thiophene fragment, the peak at  $1642\text{ cm}^{-1}$  is assigned to the C=N of thiazolothiazole-based units, and the bands at 1588, 1532, and  $1462\text{ cm}^{-1}$  are attributed to the stretching vibrations of C=C in the thiophene ring. The peaks at 1192, 1084 and  $1036\text{ cm}^{-1}$  imply in-plane C-H bending vibrations, while the out-of-plane C-H bending vibration has been assigned to the bands found in the range of  $710\text{--}1004\text{ cm}^{-1}$ . The  $866\text{ cm}^{-1}$  band is assigned to the C-S stretching vibration in the thiophene ring. By contrast, the C-H stretching vibrations of the  $2964\text{ cm}^{-1}$  band obviously became weaker, the stretching vibrations of C=N shift to  $1655\text{ cm}^{-1}$ , while the asymmetric and symmetric stretching vibrations of C=C from 1462 and  $1588\text{ cm}^{-1}$  to 1472 and  $1634\text{ cm}^{-1}$  signify a change in the C=C bond after the reaction [35], indicating the formation of the PolyDTTF polymer. Moreover, a series of peak spectral bands in the range of  $740\text{--}1094\text{ cm}^{-1}$  disappeared in the PolyDTTF, which was probably related to the electropolymerization of PolyDTTF transforming the C-H groups to form conjugate

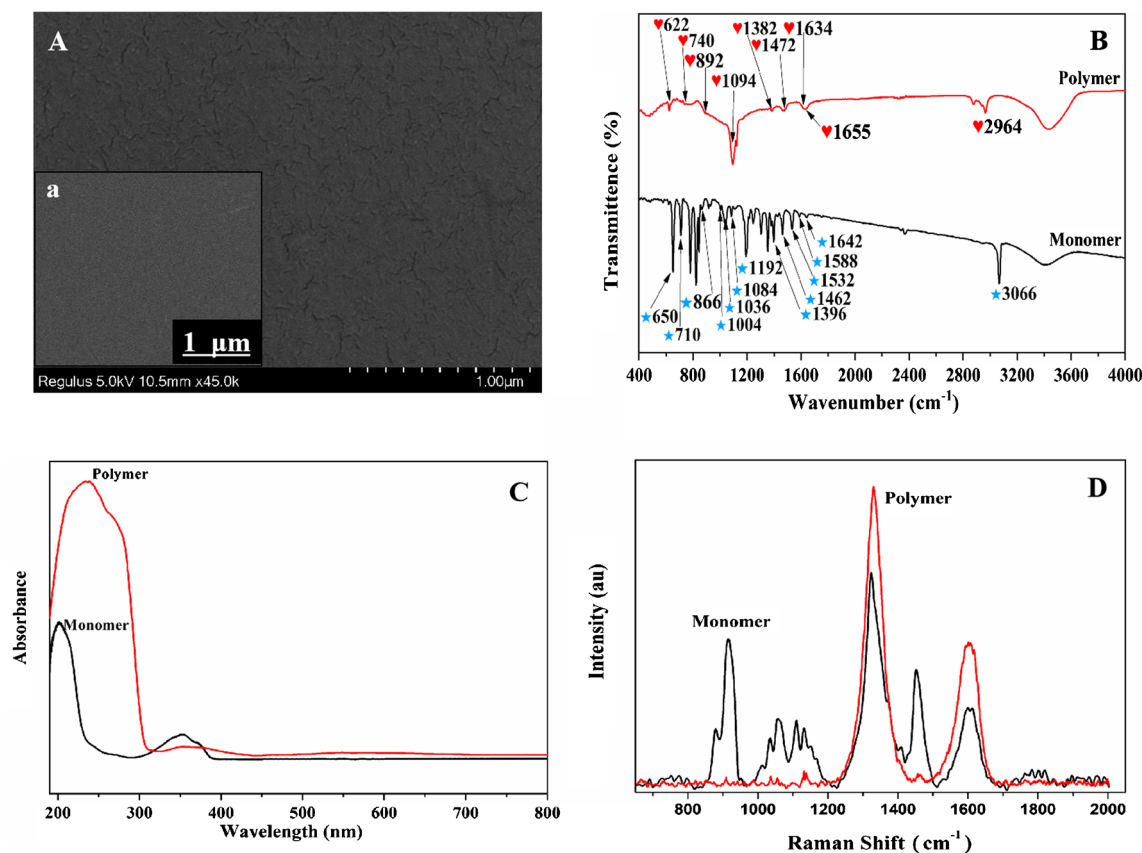


**Fig. 1** SEM images of bare GCE (a) and the polymer film (a), FT-IR spectra (b), UV-visible spectra (c), Raman spectrum (d) of the monomer and polymer film

units as a result of the relocation of  $\pi$  electrons. Furthermore, the appearance of the 892 cm<sup>-1</sup> band also represents the C-S stretching vibration in PolyDTTF, and the shift from the 650 cm<sup>-1</sup> peak to the 622 cm<sup>-1</sup> peak band reveals the ring deformation of C-S-C in the conducting polymer, further confirming the successful preparation of the polymer [22, 35].

The UV absorption spectra of the DTT and PolyDTTF were studied and shown in Fig. 1c. Compared with DTT monomer, a red-shift at the main band and the shoulder of PolyDTTF in the region of 200–310 nm can be obviously observed, which may be associated with a longer conjugation length in the PolyDTTF. It is expected that PolyDTTF has extra electron-rich rings on the backbone of the polymer and forms more extended delocalization of  $\pi$ -electron systems, which results in increased interaction between adjacent molecules in PolyDTTF. It also displays two weak absorption bands in the 330–420 nm and 480–630 nm regions [36, 37], which are attributed to the charge transfer between the donor intramolecular units (thiophene) and the thiazolothiazole-based units.

The in situ Raman spectra of DTT and PolyDTTF are revealed in Fig. 1d. Relative to the monomer, a series of peak spectral bands in the range of 1230–1650 cm<sup>-1</sup> for the polymer have varying degrees of intensity changes. Among them,

the peak bands in the range of 1510–1650 cm<sup>-1</sup> are assigned to the C=C and C=N vibrations of the thiophene fragments and thiazolothiazole-based units, the peak bands appearing at 1333 cm<sup>-1</sup> correspond to the vibration of C-C bonds. By contrast, the two bands at 926 and 827 cm<sup>-1</sup> for DTT are attributed to C-H in- and out-of-plane deformations, while these peaks disappeared in the PolyDTTF, indicating that almost all the C-H groups have been transformed into conjugate units in PolyDTTF by polymerization. The observed broadening and red shift could be on account of the variation of conjugation length distribution in the PolyDTTF [34].

### CV and EIS characterization

The electrochemical characteristics of the working electrode were investigated through cyclic voltammetry and electrochemical impedance spectroscopy. Figure 2a revealed the cyclic voltammograms of different electrodes in 0.1 M pH 7.0 PBS, containing 2.0 mM K<sub>3</sub>Fe(CN)<sub>6</sub> and 0.1 M KCl, the current of the PolyDTTF/GCE (curve b) is smaller than that of bare GCE (curve a), suggesting the successful construction of the modified electrode.

In Fig. 2b, EIS was carried out to further study the modified electrode interface with a standard redox probe i.e. Fe(CN)<sub>6</sub><sup>3-</sup>

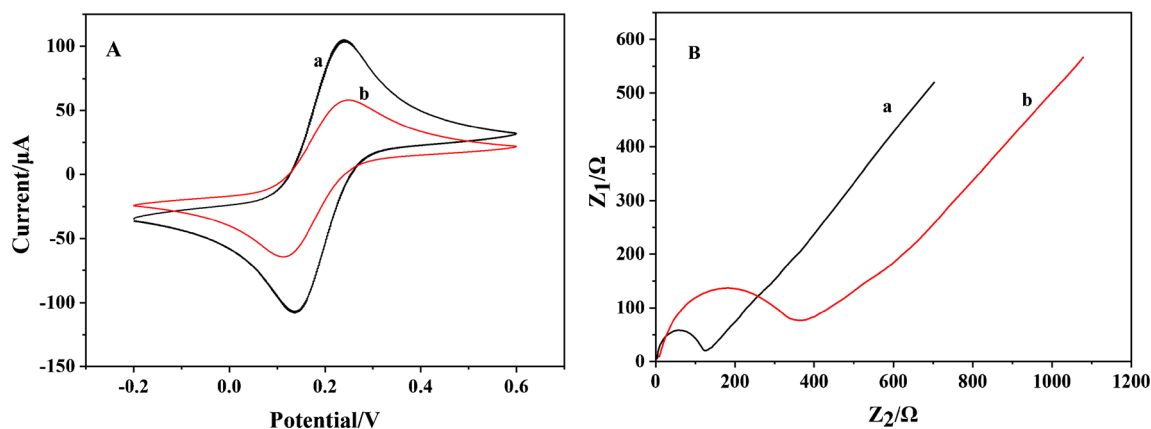


**Fig. 2** a CV curves of (a) bare GCE and (b) PolyDTTF/GCE in 0.1 M PBS solution containing 2.0 mM  $K_3Fe(CN)_6$  and 0.1 M KCl at 0.1 V/s; b EIS of (a) bare GCE and (b) PolyDTTF/GCE in 0.1 M PBS solution containing 0.1 M KCl and 5.0 mM  $[Fe(CN)_6]^{3-/4-}$

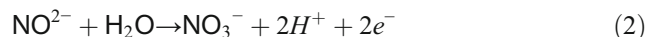
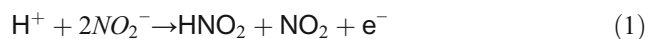
$^{-/4-}$ , as well as KCl as supporting electrolyte. A remarkable increase in the semicircle diameter of the modified electrode was observed compared with GCE (curve b), that is, the charge transfer resistance of the modified electrode is larger than that of the bare electrode, which were in accordance with the CV results. All these further indicate that PolyDTTF film has been fully loaded on the surface of the electrode.

### Electrochemical properties of DTT conductive polymer

The electrodeposition process for conductive PolyDTTF has been shown in Fig. 3a, from which, it can be found that the current gradually slows down and tends to be stable, which shows that PolyDTTF gradually reaches a saturation state on the electrode; that is, PolyDTTF has been successfully prepared on the electrode surface.

The electrochemical behavior of the bare GCE and PolyDTTF/GCE in PBS with and without nitrite was investigated by using CV. As represented in Fig. 3b, when the electrode measured the current in the nitrite solution at a sweep speed of 0.1 V/s (pH 5.0), a large oxidation peak appeared in the vicinity of 0.85–0.95 V. When the electrodes were in

0.1 M PBS solution without nitrite, there was no current response for both the bare electrode (curve a) and the modified electrode (curve b), while a significant increase in the signal of the oxidation peak current was observed for both the bare electrode (curve c) and the modified electrode (curve d) in 0.1 M nitrite solution. Moreover, the response current of the modified electrode is much better than that of the GCE in nitrite solution. Therefore, it can be concluded that PolyDTTF has excellent electrocatalytic properties towards the oxidation of nitrite. The mechanism of electro-oxidation of nitrite can be expressed as follows [30, 38]:



To further assess the electro-oxidation behavior of nitrite at PolyDTTF/GCE, we examined the CVs of different scan rates in 0.1 M pH 5.0 nitrite solution. Figure 4 depicts the corresponding increase in peak current as the scan rate increases from 0.5 V/s to 2.5 V/s. A proportional relationship between peak current and the square root of the scan rate can be observed in the illustration, and the fitted linear curve can be

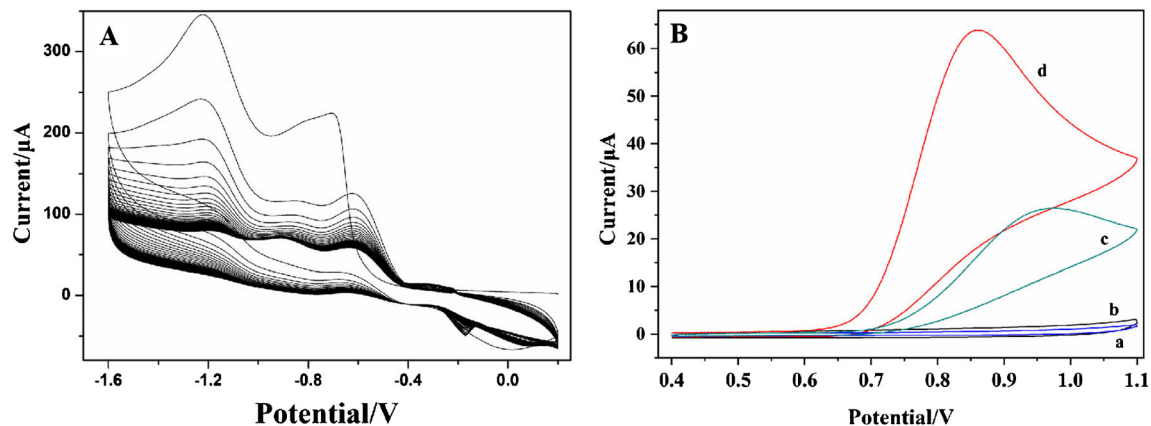


**Fig. 3** a Electrodeposition of the polymer film in acetonitrile solution containing 0.06 g/mL DTT; b CVs at different electrodes in 0.1 M PBS solution without (a, b) or with (c, d) 0.1 M nitrite. Scan rate: 0.1 V/s. a and c: bare GCE; b and d: PolyDTTF/GCE



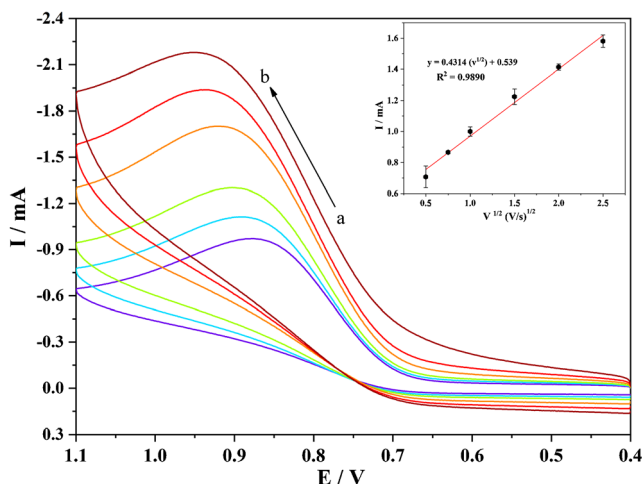


**Fig. 4** CVs of modified electrode at various scan rates in 0.1 M (pH 5.0) nitrite. (from a to b: 0.5, 0.75, 1.0, 1.5, 2.0 and 2.5 V/s). The linear relationship between current signals and the scan rate

expressed as  $y = 0.4314v^{1/2} + 0.5390$  ( $R^2 = 0.9890$ ), which indicates that the electrochemical oxidation of nitrite on PolyDTTF/GCE is a diffusion-controlled process.

### Optimization of nitrite detection conditions

To improve the performance of the sensor, we performed amperometric titration by measuring the electrochemical behavior at different pH values. Our analysis revealed that the maximum current response of nitrite increased as the solution pH increased from 4 to 5, when the pH of the solution was higher than 5.0, the peak oxidation current gradually decreased. The decrease in the oxidation peak current at low pH (<5.0) may be due to the protonation of nitrite, while the reduction in current observed at high pH (>5.0) is owing to the deficiency of the protons in the system, and that the kinetic control reduces the oxidation peak current of nitrite on the PolyDTTF/GCE [30]. Therefore, 0.1 M PBS (pH = 5) was used as the electrolyte for all electrochemical measurements.

The number of scanning turns for electrodeposition is another important factor in the detection of nitrite by the sensor. Electrodeposition processes were recorded in solutions with different scanning turns, however, the peak current has shown significant variation with the scanning turns of the solution. The results showed that the peak current increases at first and then decreases with the increase of the scanning circles number. Moreover, the maximum current signal response occurred when the number of scanning circles is 35. Hence, a scanning turn count of 35 was used as the best condition for the subsequent studies.

The electrochemical behavior of nitrite ions also depends on the sweep speed of electrodeposition. Therefore, we used I-t curves to study the electrochemical behavior at different sweep speeds (Fig. 5a). As the sweep rate increases, the peak potential of the nitrite ion-catalyzed oxidation shifts toward the corrected potential, suggesting a kinetic limit to the reaction between the redox site of the modifier and the nitrite ion [39]. Based on the oxidation peak current signal, the response is greatest at a sweep rate of 1.0 V/s. Consequently, the optimal sweep rate of 1.0 V/s was chosen for the experimental determination.

The I-t curves of nitrite on modified electrodes at different applied potentials were also investigated under optimal conditions. As represented in Fig. 5b, the peak current of nitrite increased with increasing potential from 0.6 V to 0.9 V, and then the peak current reduced significantly with the increase in the potential, thereby the potential of 0.9 V was used as an optimum value in all further studies.

### Amperometric detection of nitrite on DTT conductive polymers

Under the optimal conditions, the nitrite solutions with different concentrations were titrated by the I-t curve, and the relationship between nitrite oxidation peak concentration and current was studied. In Fig. 6a, it can be found that with the

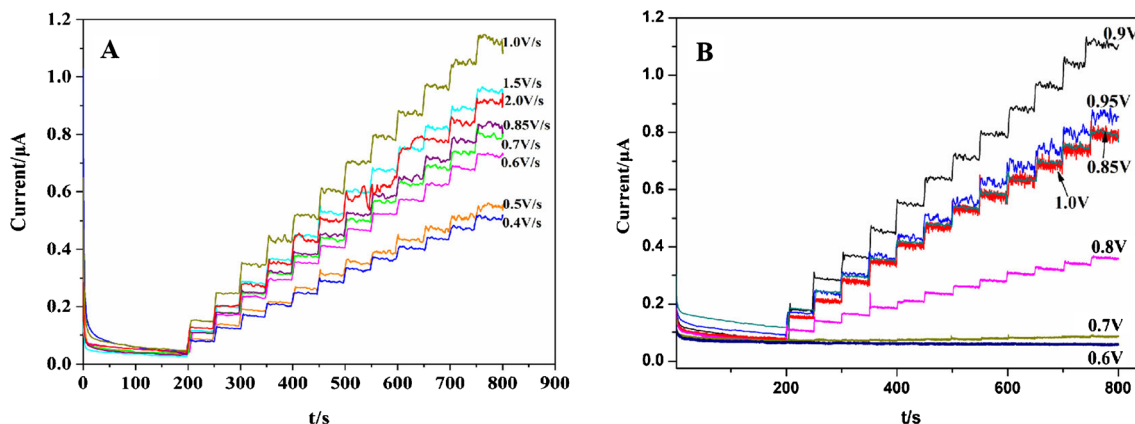


**Fig. 5** Effects of (a) sweep speeds (0.4, 0.5, 0.6, 0.7, 0.85, 1.0, 1.5, 2.0 V/s) and (b) applied potentials (0.6, 0.7, 0.8, 0.85, 0.9, 0.95, 1.0 V) on the current response of the sensor

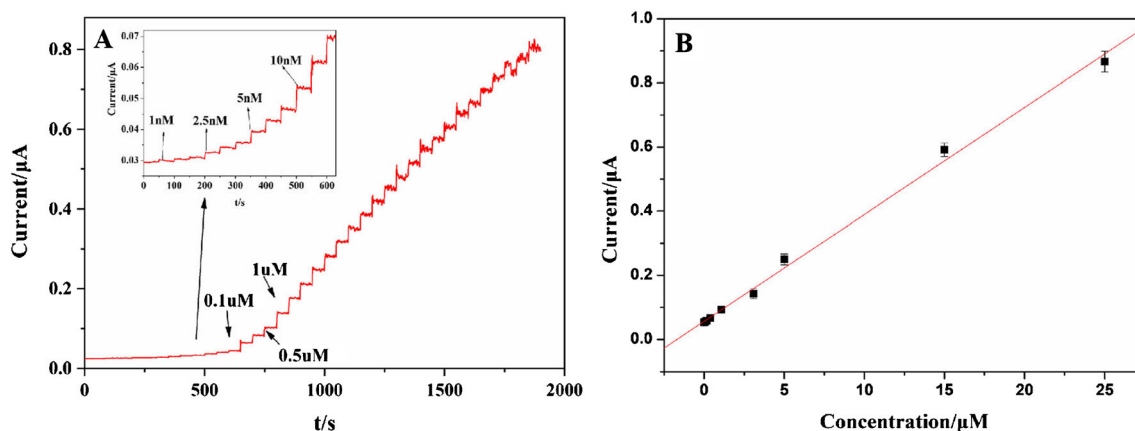


**Fig. 6** **a** Amperometric I-t curve response obtained at PolyDTTF/GCE upon successive addition of nitrite in 0.1 M PBS (pH 5.0) at 0.9 V under a constant-rate stirring condition. **b** Corresponding calibration curves

addition of a series of sodium nitrite by using different concentrations, the I-t curve sensitively exhibits apparent current step. As represented in Fig. 6b, the current response signal was plotted with increasing concentration of nitrite in the range of  $5.5 \times 10^{-9} \sim 3.5 \times 10^{-5}$  M. The modified electrode displayed wide linearity; the linear regression equation was  $Y = 0.033X + 0.0545$  with a correlation coefficient of 0.9972; the detection limit is calculated to be 2 nM. The results show that the nitrite sensor has high sensitivity for the determination of nitrite.

A comparison of analytical performance for the sensor with other reported sensors for the nitrite determination is presented in Table 1, where our modified electrode exhibited better performance as compared with other sensors, with a particularly remarkable detection limit and presentable linear region. This is mainly attributed to the high electron affinity and the synergistic effect of PolyDTTF, which could meet the requirements of rapid adsorption of analyte to the electrode surface and distinguish among them. Furthermore, PolyDTTF has good electrical conductivity and offers enhanced electrocatalytic activity, which greatly heightens the electron transfer

**Table 1** Comparison of the proposed sensor with other reported methods

Modifier	Linear range ( $\mu\text{M}$ )	Detection limit ( $\mu\text{M}$ )	Reference
CuO/H-C <sub>3</sub> N <sub>4</sub> /rGO	0.2–110	0.016	[19]
CU/MWCNT/Gr	0.005–0.36	0.30	[40]
SC-MoS <sub>2</sub>	0.006–4.2	2.0	[41]
rGO/Pd nanocomposite	0.04–0.536	15.64	[42]
AuNPs/GO-SH	0.005–1.0	0.25	[43]
AuNPs/PANI/SnO <sub>2</sub>	0.00025–2.4	0.08	[44]
MoS <sub>2</sub> -MWCNTs-Au	0.012–6.5	4.0	[45]
PolyDTTF/GCE	0.0055–35	0.002	Present work

between the amperometric responses and the nitrite concentration for three replicate measurements

kinetics and facilitates electron transfer for nitrite ion detection. As well, it is worth noting that the fabrication of the established electrode is more controllable, more reliable and easier than most reported electrochemical sensors.

### Selectivity and stability of the nitrite sensing platform

The interference experiment of nitrite detection was performed and the selectivity of the sensor was evaluated, the effect of the possible interfering anions and cations (1 M) were studied in presence of 1 mM nitrite concentration, such as NiCl<sub>2</sub>, Cu(NO<sub>3</sub>)<sub>2</sub>, NH<sub>4</sub>Cl, GaCl<sub>2</sub>, NaAc, KCl, NaH<sub>2</sub>PO<sub>4</sub>, KBr. As shown in Fig. S3 (see Electronic Supplementary Material Fig. S3), the modified electrode exhibits a remarkable response towards NaNO<sub>2</sub>, while there are no signal changes for the interfering species, showing that the prepared sensor possesses good selectivity and anti-interference ability for nitrite determination. In addition, the long-term stability of the modified GCE was investigated by detecting the current response at different intervals of time: the response signal still retained 97% and 91% of the initial response signal within three days and twenty days, respectively, which fully demonstrates that the nitrite sensor has satisfactory stability and repeatability.

**Table 2** Detection of nitrite in actual samples

Sample	The proposed sensor ( $\mu\text{g/g}$ )	The reference method ( $\mu\text{g/g}$ )	Relative deviation (%)
Ham	2.45	2.37	-3.4%
Sauce beef	0.398	0.405	1.7%
Pickles	5.18	5.29	2.1%

## Measurement and analysis of actual samples

In order to explore the feasibility of the fabricated sensor in practical applications, the PolyDTTF-modified electrode was verified by testing the nitrite content in actual samples such as ham, sauce beef, and pickle sample extracts, and compared with the traditional titration method. In Table 2, the results revealed that the relative error of two methods ranged from  $-3.4\%$  to  $2.1\%$ , with no significant difference between these two methods, indicating the practical feasibility of the sensor for nitrite detection in real samples.

## Conclusion

In brief, a novel electrochemical sensing platform was established based on PolyDTTF through one-step electropolymerization, which was applied for nitrite sensing. The as-prepared sensor showed prominent electrocatalytic activity on the electro-oxidation of nitrite. Amperometric determination demonstrates that the proposed method not only possesses a wide linear range, high sensitivity, fast response time, and low detection limit, but also provides high selectivity and good stability for nitrite detection. More importantly, it could be successfully utilized for nitrite quantification in actual samples, revealing a promising potential application in the food industry and environmental analysis.

**Supplementary Information** The online version contains supplementary material available at <https://doi.org/10.1007/s00216-021-03630-y>.

**Acknowledgments** We are deeply grateful for the support of National Natural Science Foundation of China (No. 21705084), the Natural Science Foundation of Shandong Province of China (No. ZR2017BB074), National Training Program of Innovation and Entrepreneurship for Undergraduates (No. S202010431027), Qilu University of Technology of Training Program of Innovation and Entrepreneurship for Undergraduates (No. xj201910431125), the Innovation Team of Jinan City (2018GXRC004), and Special Funds for Taishan Scholars Project.

## Declarations

**Conflict of interest** The authors have read the policy on conflicts of interest and declare no competing interests with other people or organizations.

## References

- Fan Z, Ding Z, Zhang X, Wu S, Wang M, Tong Z. Construction of cobalt porphyrin/strontium tantalite nanocomposite as a novel sensor for the detection of nitrite. *Mater Lett*. 2019;253:281–4. <https://doi.org/10.1016/j.matlet.2019.06.088>.
- Chen H, Yang T, Liu F, Li W. Electrodeposition of gold nanoparticles on Cu-based metal-organic framework for the electrochemical detection of nitrite. *Sens Actuators B-Chem*. 2019;286:401–7. <https://doi.org/10.1016/j.snb.2018.10.036>.
- Diouf A, El Bari N, Bouchikhi B. A novel electrochemical sensor based on ion imprinted polymer and gold nanomaterials for nitrite ion analysis in exhaled breath condensate. *Talanta*. 2020;209:120577. <https://doi.org/10.1016/j.talanta.2019.120577>.
- Lete C, Chelu M, Marin M, Mihaiu S, Preda S, Anastasescu M, et al. Nitrite electrochemical sensing platform based on tin oxide films. *Sens Actuators B-Chem*. 2020;316:128102. <https://doi.org/10.1016/j.snb.2020.128102>.
- Sahoo S, Sahoo PK, Sharma A, Satpati AK. Interfacial polymerized RGO/MnFe<sub>2</sub>O<sub>4</sub>/polyaniline fibrous nanocomposite supported glassy carbon electrode for selective and ultrasensitive detection of nitrite. *Sens Actuators B-Chem*. 2020;309:127763. <https://doi.org/10.1016/j.snb.2020.127763>.
- Vishnuvardhan V, Kala R, Prasada RT. Chemical switch based reusable dual optoelectronic sensor for nitrite. *Anal Chim Acta*. 2008;623(1):53–8. <https://doi.org/10.1016/j.aca.2008.05.075>.
- Altunay N, Gürkan R, Olgaç E. Development of a new methodology for indirect determination of nitrite, nitrate, and Total nitrite in the selected two groups of foods by spectrophotometry. *Food Anal Methods*. 2017;10(7):2194–206. <https://doi.org/10.1007/s12161-016-0789-7>.
- Bru M, Burguete MI, Galindo F, Luis SV, Marín MJ, Vígara L. Cross-linked poly(2-hydroxyethylmethacrylate) films doped with 1,2-diaminoanthraquinone (DAQ) as efficient materials for the colorimetric sensing of nitric oxide and nitrite anion. *Tetrahedron Lett*. 2006;47(11):1787–91. <https://doi.org/10.1016/j.tetlet.2006.01.030>.
- Shariati-Rad M, Irandoust M, Mohammadi S. Spectrophotometric determination of nitrite in soil and water using cefixime and central composite design. *Spectrochim Acta A Mol Biomol Spectrosc*. 2015;149:190–5. <https://doi.org/10.1016/j.saa.2015.04.083>.
- Lin B, Xu J, Lin K, Li M, Lu M. Low-cost automatic sensor for in situ colorimetric detection of phosphate and nitrite in agricultural water. *ACS Sens*. 2018;3(12):2541–9. <https://doi.org/10.1021/acssensors.8b00781>.
- Freitas CB, Moreira RC, de Oliveira Tavares MG, Coltro WKT. Monitoring of nitrite, nitrate, chloride and sulfate in environmental samples using electrophoresis microchips coupled with contactless conductivity detection. *Talanta*. 2016;147:335–41. <https://doi.org/10.1016/j.talanta.2015.09.075>.
- Della Betta F, Vitali L, Fett R, Costa ACO. Development and validation of a sub-minute capillary zone electrophoresis method for determination of nitrate and nitrite in baby foods. *Talanta*. 2014;122:23–9. <https://doi.org/10.1016/j.talanta.2014.01.006>.
- Martínková E, Kržek T, Coufal P. Determination of nitrites and nitrates in drinking water using capillary electrophoresis. *Chem Pap*. 2014;68(8):1008–14. <https://doi.org/10.2478/s11696-014-0548-4>.
- Chamandust S, Mehrasebi MR, Kamali K, Solgi R, Taran J, Nazari F, et al. Simultaneous determination of nitrite and nitrate in Milk samples by ion chromatography method and estimation of dietary intake. *Int J Food Prop*. 2016;19(9):1983–93. <https://doi.org/10.1080/10942912.2015.1091007>.
- Lopez-Moreno C, Perez IV, Urbano AM. Development and validation of an ionic chromatography method for the determination of nitrate, nitrite and chloride in meat. *Food Chem*. 2016;194:687–94. <https://doi.org/10.1016/j.foodchem.2015.08.017>.
- Kodamatani H, Yamazaki S, Saito K, Tomiyasu T, Komatsu Y. Selective determination method for measurement of nitrite and nitrate in water samples using high-performance liquid chromatography with post-column photochemical reaction and chemiluminescence detection. *J Chromatogr A*. 2009;1216(15):3163–7. <https://doi.org/10.1016/j.chroma.2009.01.096>.



17. Lin Z, Dou X, Li H, Ma Y, Lin J-M. Nitrite sensing based on the carbon dots-enhanced chemiluminescence from peroxynitrous acid and carbonate. *Talanta*. 2015;132:457–62. <https://doi.org/10.1016/j.talanta.2014.09.046>.
18. Wu J, Wang X, Lin Y, Zheng Y, Lin J-M. Peroxynitrous-acid-induced chemiluminescence detection of nitrite based on microfluidic chip. *Talanta*. 2016;154:73–9. <https://doi.org/10.1016/j.talanta.2016.03.062>.
19. Li Y, Cheng C, Yang Y, Dun X, Gao J, Jin X-J. A novel electrochemical sensor based on CuO/H-C3N4/rGO nanocomposite for efficient electrochemical sensing nitrite. *J Alloys Compd*. 2019;798:764–72. <https://doi.org/10.1016/j.jallcom.2019.05.137>.
20. Liu Z, Manikandan VS, Chen A. Recent advances in nanomaterial-based electrochemical sensing of nitric oxide and nitrite for biomedical and food research. *Curr Opin in Electrochem*. 2019;16:127–33. <https://doi.org/10.1016/j.coelec.2019.05.013>.
21. Jilani BS, Mounesh MP, Mruthyunjayachari CD, Reddy KRV. Cobalt (II) tetra methyl-quinoline oxy bridged phthalocyanine carbon nano particles modified glassy carbon electrode for sensing nitrite: A voltammetric study. *Mater Chem Phys*. 2020;239:121920. <https://doi.org/10.1016/j.matchemphys.2019.121920>.
22. Suma BP, Adarakatti PS, Kempahanumakkagari SK, Malingappa P. A new polyoxometalate/rGO/Pani composite modified electrode for electrochemical sensing of nitrite and its application to food and environmental samples. *Mater Chem Phys*. 2019;229:269–78. <https://doi.org/10.1016/j.matchemphys.2019.02.087>.
23. Lei W, Si W, Xu Y, Gu Z, Hao Q. Conducting polymer composites with graphene for use in chemical sensors and biosensors. *Microchim Acta*. 2014;181(7):707–22. <https://doi.org/10.1007/s00604-014-1160-6>.
24. Li X. Graphene-TiO<sub>2</sub> nanocomposite-modified screen-printed electrode for sensitive nitrite determination in hot spring water. *Int J Electrochem Sci*. 2018;13:315–23. <https://doi.org/10.20964/2018.01.38>.
25. Velmurugan S, Palanisamy S, Yang TCK. Single-crystalline SnS<sub>2</sub> nano-hexagons based non-enzymatic electrochemical sensor for detection of carcinogenic nitrite in food samples. *Sens Actuators B-Chem*. 2020;316:128106. <https://doi.org/10.1016/j.snb.2020.128106>.
26. Hu J, Zhang J, Zhao Z, Liu J, Shi J, Li G, et al. Synthesis and electrochemical properties of rGO-MoS<sub>2</sub> heterostructures for highly sensitive nitrite detection. *Ionics*. 2018;24(2):577–87. <https://doi.org/10.1007/s11581-017-2202-y>.
27. Gholivand M-B, Jalalvand AR, Goicoechea HC. Computer-assisted electrochemical fabrication of a highly selective and sensitive amperometric nitrite sensor based on surface decoration of electrochemically reduced graphene oxide nanosheets with CoNi bimetallic alloy nanoparticles. *Mater Sci Eng C*. 2014;40:109–20. <https://doi.org/10.1016/j.msec.2014.03.044>.
28. Deng K, Zhou J, Huang H, Ling Y, Li C. Electrochemical determination of nitrite using a reduced graphene oxide–multiwalled carbon nanotube-modified glassy carbon electrode. *Anal Lett*. 2016;49(18):2917–30. <https://doi.org/10.1080/00032719.2016.1163364>.
29. Wang Y, Bi C-y. a novel nitrite biosensor based on direct electron transfer of hemoglobin immobilized on a graphene oxide/au nanoparticles/multiwalled carbon nanotubes nanocomposite film. *RSC Adv*. 2014;4(60):31573–80. <https://doi.org/10.1039/C4RA05237D>.
30. Zhang S, Tang Y, Chen Y, Zheng J. Synthesis of gold nanoparticles coated on flower-like MoS<sub>2</sub> microsphere and their application for electrochemical nitrite sensing. *J Electroanal Chem*. 2019;839:195–201. <https://doi.org/10.1016/j.jelechem.2019.03.036>.
31. Cosnier S, Holzinger M. Electrosynthesized polymers for biosensing. *Chem Soc Rev*. 2011;40(5):2146–56. <https://doi.org/10.1039/C0CS00090F>.
32. Reginato G, Mordini A, Zani L, Calamante M, Dessì A. Photoactive compounds based on the Thiazolo[5,4-d]thiazole Core and their application in organic and hybrid photovoltaics. *Eur J Org Chem*. 2016;2016(2):233–51. <https://doi.org/10.1002/ejoc.201501237>.
33. Jung IH, Yu J, Jeong E, Kim J, Kwon S, Kong H, et al. Synthesis and photovoltaic properties of Cyclopentadithiophene-based low-bandgap copolymers that contain Electron-withdrawing Thiazole derivatives. *Chem-Eur J*. 2010;16(12):3743–52. <https://doi.org/10.1002/chem.200903064>.
34. Ahumada JC, Leyton P, Aristizabal JA, Soto JP. Synthesis and morphological characterization of a new conjugated polymer based on benzobisoxazole and thiophene systems. *Polym Bull*. 2018;75(2):597–610. <https://doi.org/10.1007/s00289-017-2057-4>.
35. Zhang X-C, Wu S-H, Jia S-Y, Wang C, Sun S-W, Wang X-M, et al. Turning thiophene contaminant into polymers from wastewater by persulfate and CuO. *Chem Eng J*. 2020;397:125351. <https://doi.org/10.1016/j.cej.2020.125351>.
36. Bevk D, Marin L, Lutsen L, Vanderzande D, Maes W. Thiazolo[5,4-d]thiazoles – promising building blocks in the synthesis of semiconductors for plastic electronics. *RSC Adv*. 2013;3(29):11418–31. <https://doi.org/10.1039/C3RA40851E>.
37. Dağcı K, Alanyaloğlu M. Electrochemical preparation of polymeric films of pyronin Y and its electrocatalytic properties for amperometric detection of nitrite. *J Electroanal Chem*. 2013;711:17–24. <https://doi.org/10.1016/j.jelechem.2013.10.016>.
38. Ghanei-Motlagh M, Taher MA. A novel electrochemical sensor based on silver/halloysite nanotube/molybdenum disulfide nanocomposite for efficient nitrite sensing. *Biosens Bioelectron*. 2018;109:279–85. <https://doi.org/10.1016/j.bios.2018.02.057>.
39. Kamyabi MA, Aghajanloo F. Electrocatalytic oxidation and determination of nitrite on carbon paste electrode modified with oxovanadium(IV)-4-methyl salophen. *J Electroanal Chem*. 2008;614(1):157–65. <https://doi.org/10.1016/j.jelechem.2007.11.026>.
40. Abo-Hamad A, AlSaadi MA, Hashim MA. Eutectic mixture-functionalized carbon nanomaterials for selective amperometric detection of nitrite using modified glassy carbon electrode. *J Electroanal Chem*. 2018;812:107–14. <https://doi.org/10.1016/j.jelechem.2018.01.052>.
41. Wang H, Wen F, Chen Y, Sun T, Meng Y, Zhang Y. Electrocatalytic determination of nitrite based on straw cellulose/molybdenum sulfide nanocomposite. *Biosens Bioelectron*. 2016;85:692–7. <https://doi.org/10.1016/j.bios.2016.05.078>.
42. Zhang Y, Zhao Y, Yuan S, Wang H, He C. Electrocatalysis and detection of nitrite on a reduced graphene/Pd nanocomposite modified glassy carbon electrode. *Sens Actuators B-Chem*. 2013;185:602–7. <https://doi.org/10.1016/j.snb.2013.05.059>.
43. Pan F, Chen D, Zhuang X, Wu X, Luan F, Zhang S, et al. Fabrication of gold nanoparticles/l-cysteine functionalized graphene oxide nanocomposites and application for nitrite detection. *J Alloys Compd*. 2018;744:51–6. <https://doi.org/10.1016/j.jallcom.2018.02.053>.
44. Duan C, Bai W, Zheng J. Non-enzymatic sensors based on a glassy carbon electrode modified with au nanoparticles/polyaniline/SnO<sub>2</sub> fibrous nanocomposites for nitrite sensing. *New J Chem*. 2018;42(14):11516–24. <https://doi.org/10.1039/c8nj01461b>.
45. Zhang Y, Wen F, Tan J, Jiang C, Zhu M, Chen Y, et al. Highly efficient electrocatalytic oxidation of nitrite by electrodeposition of au nanoparticles on molybdenum sulfide and multi-walled carbon nanotubes. *J Electroanal Chem*. 2017;786:43–9. <https://doi.org/10.1016/j.jelechem.2017.01.007>.